Zeolites are no longer a challenge

Mayoral, Alvaro; Anderson, Paul; Diaz, Isabel

DOI:
10.1016/j.micron.2014.05.009

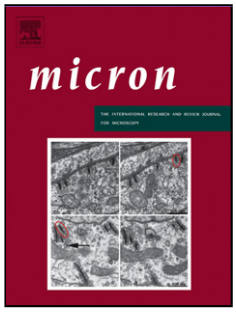

Title: Zeolites are no longer a challenge: Atomic resolution data by Aberration-corrected STEM

Author: Alvaro Mayoral Paul A. Anderson Isabel Diaz

PII: S0968-4328(14)00115-2
DOI: http://dx.doi.org/doi:10.1016/j.micron.2014.05.009
Reference: JMIC 2087

To appear in: *Micron*

Received date: 4-2-2014
Revised date: 7-5-2014
Accepted date: 24-5-2014

Please cite this article as: Mayoral, A., Anderson, P.A., Diaz, I.,Zeolites are no longer a challenge: Atomic resolution data by Aberration-corrected STEM, *Micron* (2014), http://dx.doi.org/10.1016/j.micron.2014.05.009

- Aberration corrected STEM has been successfully applied to porous solids.
- Structural defects have been analyzed with unprecedented resolution.
- All “T” atoms forming the structure can be located.
- Silver octahedra, composed of 6 atoms, have been imaged.

Zeolites are no longer a challenge: Atomic resolution data by Aberration-corrected STEM

Alvaro Mayoral[a,*], Paul A. Anderson[b], Isabel Diaz[c]

[a] Advanced Microscopy Laboratory (LMA), Nanoscience Institute of Aragon (INA), University of Zaragoza, Mariano Esquillor, Edificio I+D, 50018, Zaragoza, Spain.

[b] School of Chemistry, The University of Birmingham, Edgbaston, Birmingham B15 2TT, United Kingdom

[c] Instituto de Catalisis y Petroleoquimica, CSIC, Marie Curie, 2. 28049 Madrid (Spain)

Abstract

Transmission electron microscopy is undoubtedly an indispensable tool for materials characterization, which can currently reach sub-angstrom resolution down to the elemental building blocks of matter, isolated single atoms of most elements. In addition to the phenomenal image resolution, if the material is strong enough, it can be accompanied with chemical information, converting electron microscopy into a unique method for the analysis of a great variety of materials. Unfortunately, extracting all this valuable information is not simple as most materials in one way or another are affected by the strong and localized electron beam. Radiolysis is one kind of reaction between electrons and matter than can cause irreversible structural transformations in our materials. This effect is the predominant factor in zeolites, zeotypes and the majority of molecular sieves. In the present work some results, taken at high voltage (300 kV) and minimizing the exposure to the beam, are presented proving the feasibility of the technique to obtain unprecedented atomic resolution information of different zeolites and microporous solids.

Introduction

Transmission electron microscopy is currently an indispensable tool for characterization of any type of organic and inorganic materials, which provides a great variety of information such as lattice constants, atomic variations in the crystal structure or compositional and chemical environment among many others. Besides the invaluable information that can be obtained, the highly energetic electron beam can cause temporary or permanent damage in the specimen structure. The two main mechanisms that have been described in relation to electron beam damage inside of a transmission electron microscope (TEM) are radiolysis and knock-on damage (Egerton, 2013; Egerton et al., 2004; Egerton et al., 2010; Williams and Carter, 1996).

Knock-on damage can be explained as the displacement of the atoms forming the specimen due to the incident electrons of the incoming beam. This process could be

overcome by reducing the accelerating voltage, as for most inorganic materials there is a threshold value (Egerton et al., 2010).

Radiolysis (ionization damage) is a more effective process and results from the dissociation of chemical bonds as a result of a high energy flux onto a material and in the case of an electron microscope is composed of several electron excitations, such as inner shell ionization, plasmon loss, creation of locally bound electron–hole pairs and the cross section, which paradoxically decreases with increasing acceleration voltage and is strongly dependent on the radiolytic sensitivity of the material and the thickness of the sample. This radiolytic damage can be expressed as (Blanford and Carter, 2003; Hobbs, 1979):

$$\sigma_e = \frac{8\pi a_0^2 R_\infty^2}{mc^2} \frac{Z'}{T'_{th}\beta^2}$$

where T'_{th} is the minimum energy required to break an atomic bond and Z' is the number of electrons around the atom. Fortunately, the efficiency of the electrons hitting the sample is not of 100% and therefore not all the electrons cause bond breaking (Hobbs, 1985). Therefore, the radiolytic damage cross section σ_r, is the result of the product of σ_e and the efficiency (ζ):

$$\sigma_r = \sigma_e \, \zeta$$

which has been found to decrease when the acceleration voltage is increased (Blanford and Carter, 2003) especially for values below 100 kV.

Zeolites are crystalline aluminosilicates with general formula: $M[Al_xSi_{1-x}O_2]\cdot nH_2O$, where M is a cation that compensates each negative charge introduced by the Al units. The framework is composed of TO_4 (T = Si or Al) tetrahedra linked by oxygen bridges forming a structure of channels and/or cavities. Such a periodical array of building units and pores that confer to zeolites a high degree of crystallinity would be expected to provide a beautiful material for transmission electron microscopy studies. Unfortunately, zeolites are extremely beam sensitive which has been associated with the radiolysis procedure. For this particular case, the presence of water has been described to take part in the radiolytic mechanism; in 1980 Bursill *et al*.(Bursill et al., 1980) discussed the effect of water present in the zeolitic cavities of the zeolite A (LTA type). It was proposed that the production of ionized species, OH^- ions, would decrease the strength of the framework bonds. Later on, the effect of the presence of water was also tested on zeolite NaY (faujasite type) (Bursill et al., 1981; Csencsits and Gronsky, 1987). Therefore, a great effort has been devoted from many top scientists into the observation of zeolites especially for the significant applications that these minerals present in catalysis (mainly petroleum refining & petrochemistry), as detergents or as ion exchangers. The first results date back to 1958 where lattice

fringes were observed in faujasite mineral (Menter, 1958). Due to the difficulty of acquiring high-resolution images the initial studies by electron microscopy (EM) were performed through electron diffraction (ED) and it was not until 1972 when an EM image was used to study faults in ERI (Kokotailo et al., 1972). Later on, in the 70's but mostly from the 80's, high-resolution (HRTEM) images were beginning to be used to analyze structural parameters in zeolites (Allpress and Sanders, 1973). Since then, different papers have been published based on high-resolution transmission electron microscopy to analyze their fine structure, defects or intergrowths with exceptional high quality (Díaz et al., 2004; Díaz and Mayoral, 2011; Ruan et al., 2009; Sakamoto and Kodaira, 2013; Terasaki and Ohsuna, 1995, 2003). All the data produced over the past years has been obtained under a careful control of the electron beam current, minimizing as much as possible the exposure time in order to avoid structural damage. With the implementation of the spherical aberration (C_s) correctors, lateral resolution is not a problem any more but the increase in the number of electrons per area would have an even more detrimental effect on the analysis of these materials. For the particular case of C_s-corrected scanning transmission electron microscopy (STEM) the high current focused onto a fine spot would easily result in burning a hole in the zeolites; on the other side, the main advantage of this technique relies on all electrons being concentrated into a very fine spot and only the scanned area would be affected.

Therefore, since 2010, by having an exhaustive control of the electron beam current, new findings have been obtained on the characterization of molecular sieves. In the present manuscript, we review our own contribution providing several examples with an unprecedented resolution through C_s-corrected STEM using annular dark field detectors.

Methods

Electron Microscopy

The electron microscopy was performed using a TITAN X-FEG 60-300, operated for every experiment at 300 kV, located at the Advance Microscopy Laboratory (LMA) in the Institute of Nanoscience of Aragon. This microscope is equipped with a high brightness field emission gun to compensate for the loss of electrons caused by the monochromator (not excited for the current experiments) in the gun zone, a CEOS spherical aberration corrector for the electron probe, an EDAX EDS detector, a Fischione HAADF detector and Gatan BF and DF detectors (not used for any experiments). In every case the microscope was corrected using a gold standard sample to obtain a C_s always below 500 nm and S_3 and A_3 below 600 nm.

Beam convergence of 24.8 mrad and 17.7 mrad half-angles were used, yielding in both cases to a calculated probe size of approximately 0.7-0.8 Å. Total dwell times varied from 6 to 14 seconds depending on the magnification and beam current applied with a maximum beam current of 16 nA.

Before electron microscopy observations the sample were deeply crushed, for several minutes when necessary, using an Agatha mortar and pestle, dispersed in ethanol and placed onto lacey carbon coated copper microgrids.

Synthesis of ETS-10 (Engelhard Corporation titanosilicate)

ETS-10 was prepared by hydrothermal synthesis (Casado et al., 2009) using TiO_2-anatase (powder, 99.80 wt.%, Aldrich) as Ti source from a gel with the following molar composition: $4.6Na_2O$: 1.9 K_2O: TiO_2: 5.5 SiO_2 : $147H_2O$. This gel was added to the sodium silicate solution under continuous stirring for 30 minutes. Subsequently, the gel obtained was poured into a Teflon-lined autoclave and subjected to hydrothermal synthesis at 230°C for 24 h. The product was finally washed in deionized water and centrifuged several times, then dried at 100°C overnight.

LTA, zeolite A

Zeolite A, in its sodium form, was prepared using a verified standard synthesis for zeolite A (Robson and Lillerud., 2001) to produce a white solid with cubic morphology.

In order to produce silver loaded zeolite A (Mayoral and Anderson, 2007) the desired amount of zeolite was stirred in a solution of $AgNO_3$ (0.1M, Sigma Aldrich, 99%) at room temperature for 16 h. The milky solution obtained was filtered and washed with deionized water (1 L) to remove any salt remaining. Afterwards, the silver zeolite A was dehydrated at 425°C for 12 h under 1×10^{-6} mbar. The material was then kept under argon in a glovebox before electron microscopic examination. For this material the sample preparation was particularly quick to minimize the time that the sample was in contact with the air.

The Cd introduction was performed as follows: NaA was ion-exchanged four times in a 0.1 M aqueous solution of $Cd(NO_3)_2$ at 80°C to obtain a fully ion-exchanged $Cd_6Al_{12}Si_{12}O_{48}$. This material was evacuated for 12 h at 550°C, then heated at this temperature for 3 h, and finally heated at a rate of 30 °C h^{-1} to 750°C under vacuum and held for 48 h at this elevated temperature. After cooling to room temperature, the zeolite, still evacuated, was transferred to an inert-atmosphere glovebox. Additional Cd was introduced by heating the dehydrated CdA with Cd powder under vacuum at 500 °C for 3 days.

Results

As already mentioned, originally, observations of zeolites could not take advantage of the sub-angstrom resolution of the most advanced aberration corrected electron microscopes due to their tremendous high sensitivity with respect to the electron beam. However, in 2010 Ortalan *et al.* (Ortalan et al., 2010) determined the location of Ir atoms on ultrastable dealuminated zeolite HY. In this work low dose conditions for imaging were used (1200 $e^- Å^{-2}$) observing at atomic level the guest Ir species but not the zeolitic framework. Later on, the same group (Browning & Gates) obtained very nice results taking an alternative approach which consisted in increasing the dose up to 10^5–10^6 $e^- Å^{-2}$ and scanning the sample very fast. With this method images perpendicular to the channels of SSZ-53 (Aydin et al., 2011) were recorded observing the motion of Ir atoms. In the same manner isolated gold atoms were identified in the structure of zeolite Y (Lu et al., 2012). Moreover a year later, a very nice comparison between aberration corrected STEM and TEM in zeolite A was published by Yoshida *et* al. (Yoshida et al., 2013).

These results proved the feasibility of advanced and at the same time complicated electron microscopy methods to provide new insights about guest species in zeolites; however, atomic resolution (columns) of the framework still would be desired that would add information about structural defects, growth mechanisms and accurate location of cations within the pores.

The results presented here, rely on the application of low dose conditions in order to magnify the image as much as possible to elucidate all atomic positions. The control of the electron beam was performed by changing the crossover position in the monochromator zone allowing a continuous control of the number of electrons without practically altering the aberrations in the microscope and therefore the final resolution.

ETS-10 contains octahedrally and tetrahedrally coordinated T atoms (T=Si, and Ti) where the TiO_6 octahedra and SiO_4 tetrahedra linked by corner-sharing oxygen atoms form a three-dimensional pore system. It possesses a monoclinic structure, *C*2/*c*, with lattice parameters a = 21.00, b = 21.00, c = 14.51 Å; β = 111.128° and $\alpha = \gamma$ = 90.00°. It is well documented (Anderson et al., 1994) that this material, with great applications in catalysis, gas absorption or optical properties, exhibits a great degree of disorder with stacking faults or “double pores” in the structure (Mayoral et al., 2013b). The structure is shown in Fig. 1a; in light blue appears the Ti, in dark blue the Si and in red the oxygen bridges. Based on the higher scattering factor of Ti with respect to Si it would be expected that the Ti rich columns appear brighter than the others. Fig. 1b shows the atomic resolution data of one crystal, where the atomic columns and the pores are clearly identified. A closer look, Fig. 1c, is displayed as a thermal colored map, identifying the T atoms and measured interatomic distances (Fig. 1d). The

highest contrast corresponds to the position marked as 2 (TiO_6 octahedra) surrounded by 4 atomic columns formed by silicon (marked as 1 and 3). The simulated image is also presented to corroborate the experimental data, assuming 35 nm thickness and a probe size of 0.9 Å.

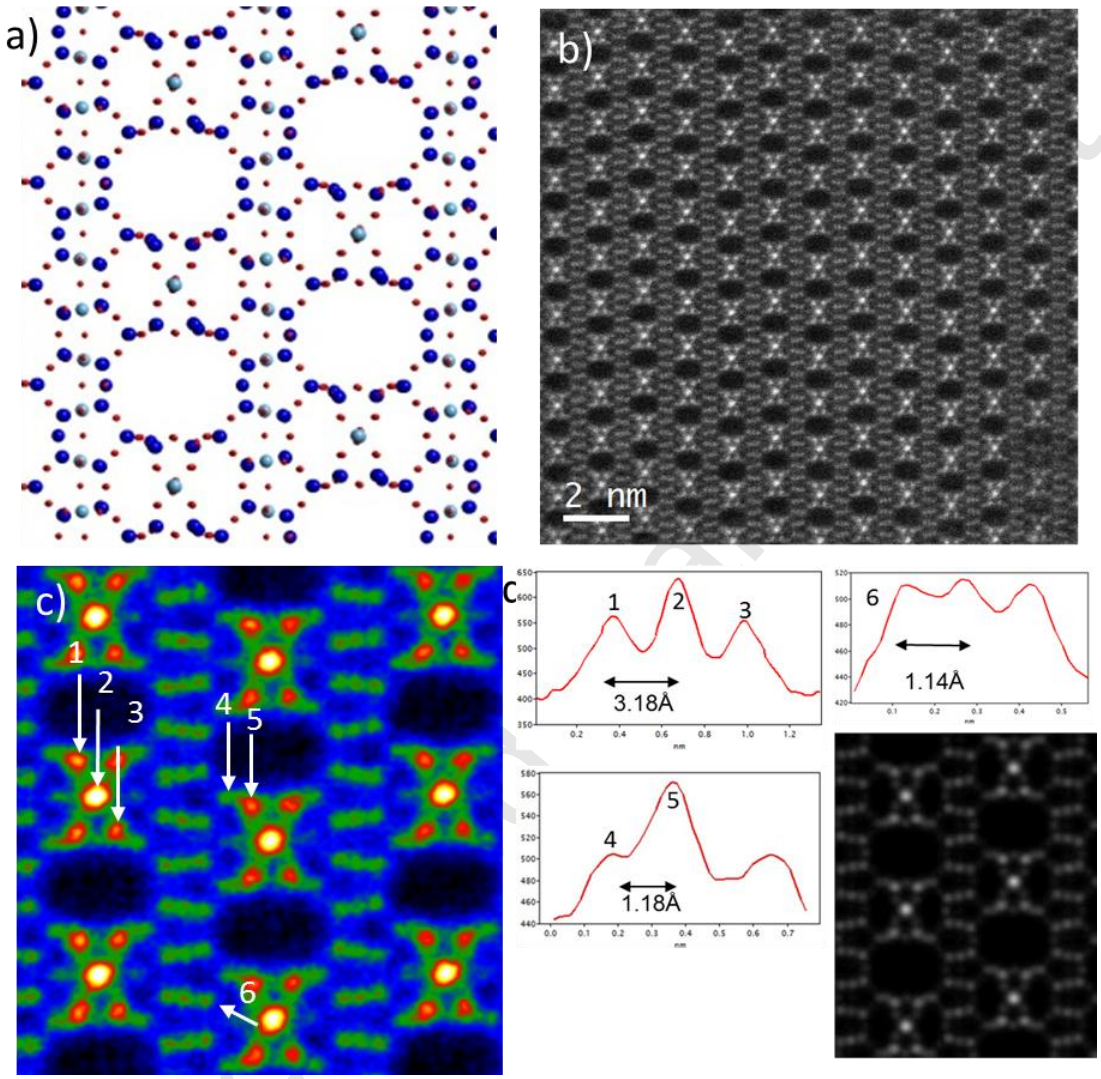

Fig 1. a) Model of ETS-10 along the [110] orientation. b) C_s-corrected STEM-HAADF image on the same orientation, where many stacking faults are observed. c) FFT filtered thermal colored map, where the different atomic columns are identified and marked with numbers. d) Intensity profiles of the positions denoted in c, together with the simulated data. Images adapted from (Mayoral et al., 2013b).

Traditionally, in these crystals the presence of the double pores in addition to the stacking disorder has been described. Fig. 2a exhibits a lower magnification image where all variations from an ideal structure are present. Faults are always present and extended over the entire crystal in every particle analyzed; however, it has to be also noted, marked by a white arrow, a lack of porosity in certain regions (always presenting

lower intensity in the images) where the octahedra and tetrahedra are connected leaving no pores between them. This configuration is actually very similar to what happens for the so-called double pores, Fig. 2b. In this case and for every crystal studied there has always been a faint signal suggesting the presence of another building unit which has not been observed by conventional TEM and "modeled" in Fig. 2c. The lower intensities observed in these defects is associated to the Si coordination number, which has to be 4. When this "lack of porosity" occurs in these new units, the Si atoms are already bonded to 4 oxygens forcing to break structure along the z axis and therefore decreasing the number of atoms in those columns giving as a result less intense signals.

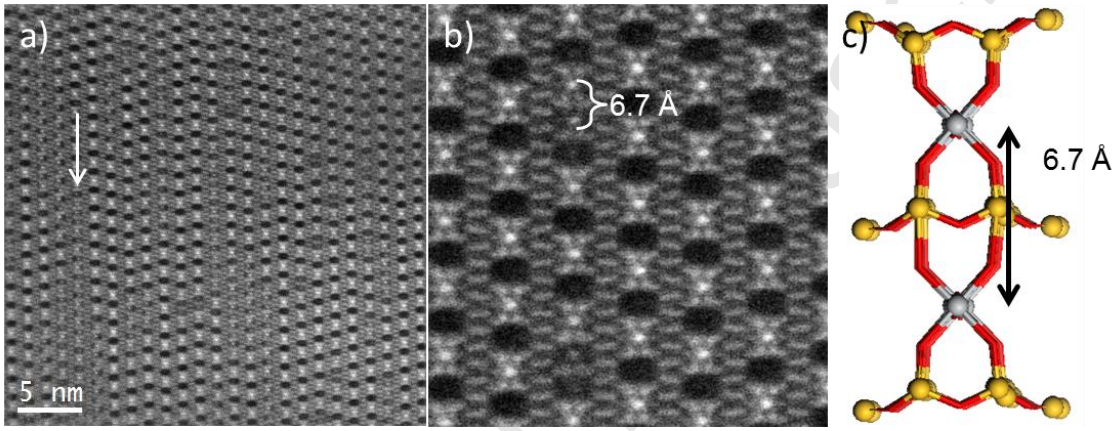

Fig.2. C_s-corrected STEM-HAADF image of a region displaying multiple intergrowths with lack of porosity, white arrow. b) Atomic-resolution image showing 2 TiO_6 units linked to each other, Ti columns separated by 6.7 Å. c) Ball and stick model resulted of linking 2 TiO_2 through SiO_4 tetrahedra.

LTA: Zeolite A presents the ideal formula $Na_{12}Al_{12}Si_{12}O_{48}$ which is the minimum Si/Al ratio possible for a zeolite making it one of the most beam sensitive zeolites due to its high Al content. However, this high ion-exchange capacity together with its structural parameters and its low cost production has led to it being the most widely industrially produced zeolite mainly for its application in detergents. Fig. 3 shows the difference in terms of resolution achieved for different beam current in the same sample. Fig. 3a displays the FFT filtered image of NaA along the [001] orientation (*Pm*-3*m* symmetry) with a beam current of hundreds of pA, meanwhile Fig. 3b shows the results when the beam current was decreased below 10 pA allowing a full identification of T atoms within the structure.

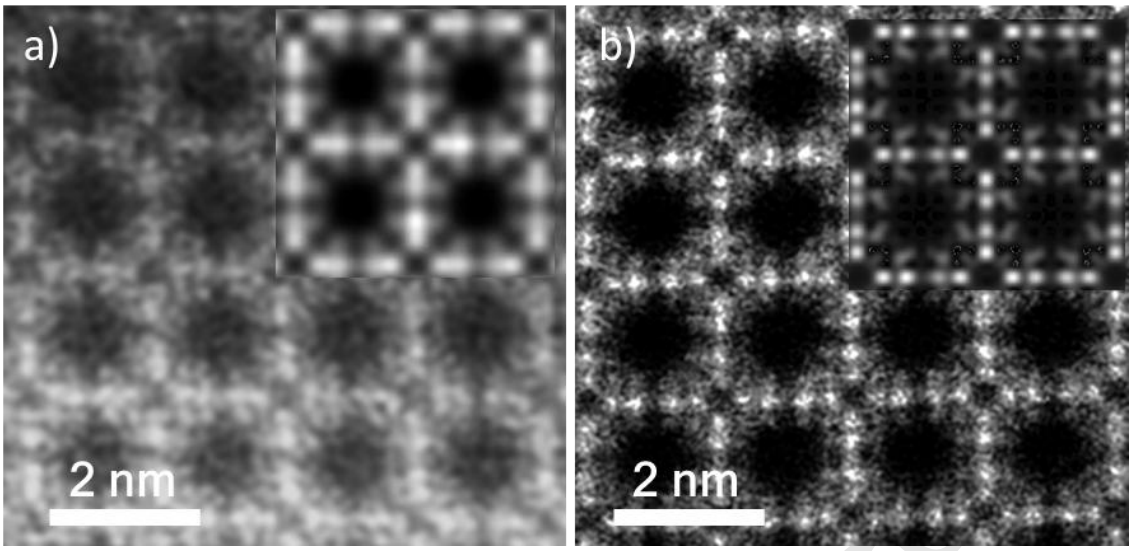

Fig. 3. C_s-corrected STEM images of NaA a) using a beam current of 150 pA, the simulated image (probe size of 1.7 Å) image adapted from (Mayoral et al., 2011), and b) using beam current of 2pA, the simulated image using a probe size of 0.7 Å.

Here the Na^+ was exchanged with Ag^+ obtaining a complete ion exchange (Mayoral et al., 2013a; Mayoral et al., 2011). After dehydration of this material the color changed from white to orange attributed to the formation of clusters in the zeolite cavities. In order to gain information on the interior of the cages the main crystallographic orientations were imaged with unprecedented resolution (Mayoral et al., 2011), Fig. 4, adapted from ref.29. A careful observation along the [001] in combination with the other orientations allowed us to resolve for the first time the silver conformation within the sodalite cages (Mayoral et al., 2011). Fig. 5a shows the Ag distribution with the sodalite cages containing 14 Ag atoms. 8 of them (4 in the projected image forming a square) forming a cube in the three dimensional space separated by 4.72 Å (Fig. 5b) containing 6 Ag more (it would be 5 in 2 dimensions) that would form the smallest octahedron ever reported. Some contrast differences can be observed inside the SOD cages which are associated to the reaction between the Ag and the O_2/H_2O from the atmosphere during sample preparation. Fig. 5c shows the model where silver appears in grey and where all interatomic distances clearly match with the experimental data measured. The intensity profiles marked in Fig. 5b are presented in Fig. 5d while the sodalite cage that contains the 9 atoms is shown in in Fig. 5e slightly tilted for better understanding.

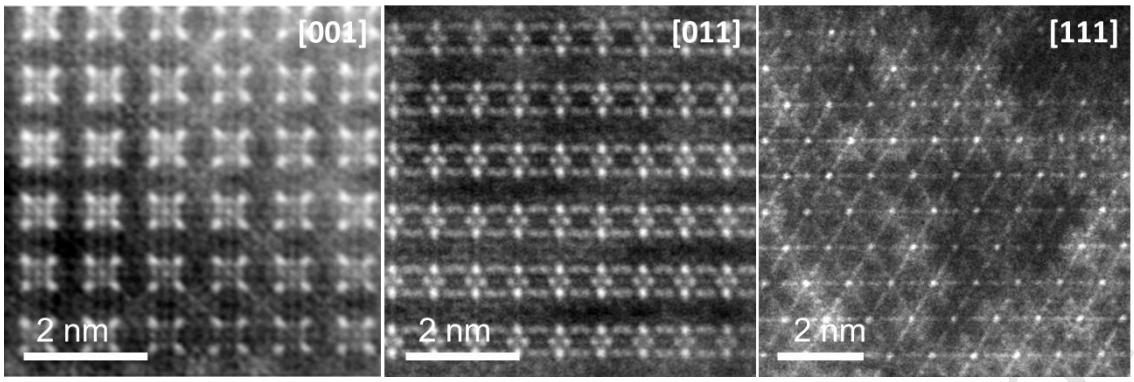

Fig. 4. C_s-corrected STEM-HAADF images of dehydrated AgA along the main crystallographic orientations, where in Ag appear as brightest atomic columns.

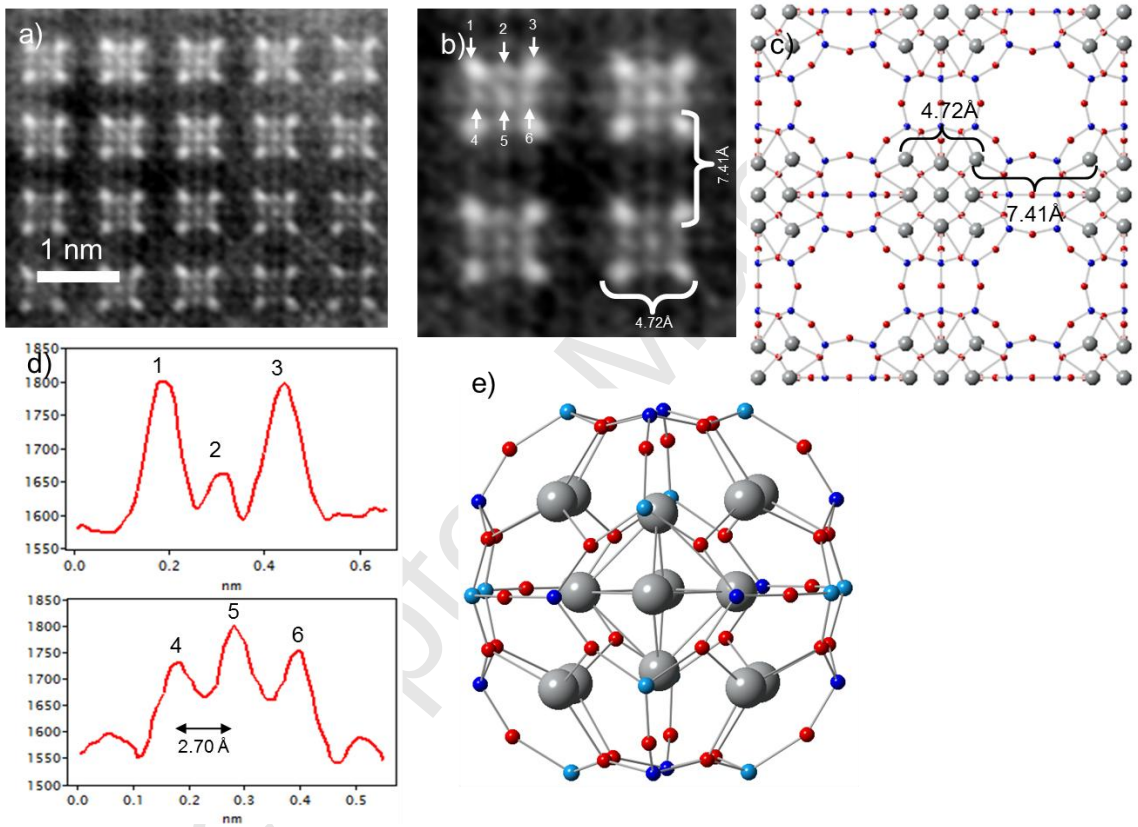

Fig. 5. a) and b) FFT filtered images of AgA along the [001]. c) Model proposed containing the Ag (in grey). d) Intensity profiles of the interatomic distances marked in b. e) Sodalite cage slightly tilted for a better visualization of the Ag.

Another good example of metals confined in the zeolite cavities is the case of CdA (Mayoral et al., 2013c). A very important application of zeolites is the ability that they have to “capture” heavy metals, as in the case of using zeolites to remove radioactive cations from water or even the human body. Cd containing zeolite A has been studied by conventional high-resolution TEM, but the metal atoms were not observed (Readman et al., 2004). Considering the stronger scattering factor of Cd with respect to

the Si, Al and O, the former should appear much brighter if observed by STEM-HAADF. A similar analysis to that previously done for silver containing zeolite A was performed for CdA recording the main crystallographic orientations ([001], [011], [111] and [211]) (Mayoral et al., 2013c). In this case, very low-dose conditions, always below than 30 pA, were used to determine how many Cd were present, their positions in the sodalite cages and their stability with respect to air and humidity. Fig 6. shows some results on the already ion-exchanged cadmium zeolite A (Si/Al = 1); a general view of a zeolite crystal is displayed in Fig 6a along the [001] observing, in a similar (but not identical) fashion to AgA, a homogenous distribution of bright spots that correspond to the Cd atomic columns. Atomic resolution information can be extracted from Fig. 6b and 6c ([001] and [011], respectively), where in addition to the Cd signals zeolite T atoms can be also identified. Cd adopts a cubic symmetry occupying the 6-rings of the sodalite cages separated by 4.11 Å; the correlation between the experimental and simulated data, see (Mayoral et al., 2013c), suggests the presence of 2 Cd species in the 6-rings.

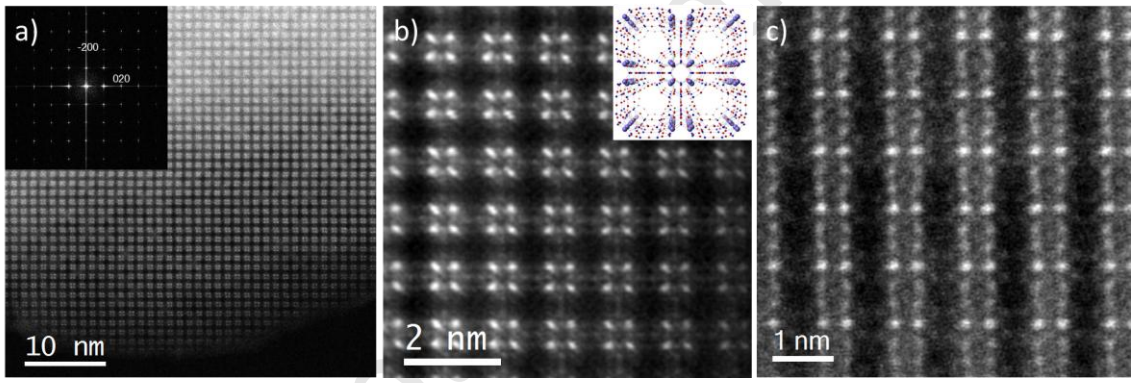

Fig.6. C_s-corrected STEM-HAADF images of Cd-containing zeolite A. a) Medium magnification image where the homogeneous distribution of Cd can be observed. The indexed FFT is shown inset. b) Atomic resolution data along the [001] with the model inset. c) CdA crystal tilted along the [011] zone axis.

Conclusions

Over the last 30 years a great effort has been devoted to the characterization of molecular sieves by transmission electron microscopy either by electron diffraction and/or by high-resolution TEM. These magnificent results have beautifully illustrated unique information on ordered porous structures such as the presence of defects, studies of the fine structures, analysis of non-periodic arrangements within the zeolites or even solving new structures. However, due to the great level of difficulty associated with the low stability of zeolites in the microscope, the most advanced instrumental techniques, i.e. spherical aberration correctors were not applied until very recently and the characterization of molecular sieves has been instrumentally stuck in the nineties.

This has dramatically changed since 2010 and nowadays any zeolite or zeotype can be imaged with atomic resolution.

Acknowledgements

A. M. thanks for funding to the European Union Seventh Framework Programme under Grant Agreement 312483 - ESTEEM2 (Integrated Infrastructure Initiative − I3). I.D. acknowledges Spanish Government for funding (MAT2012-31127).

References

Allpress, J.G., Sanders, J.V., 1973. The direct observation of the structure of real crystals by lattice imaging. J. Appl. Crystallogr. 6, 165-190.
Anderson, M.W., Terasaki, O., Oshuna, T., Philippou, A., Mackay, S.P., Ferreira, A., Rocha, J., Lidin, S., 1994. Structure of the microporous titanosilicate ETS-10. Nature 367, 347-367.
Aydin, C., Lu, J., Liang, A.J., Chen, C.-Y., Browing, N.D., Gates, B., 2011. Tracking Iridium atoms with electron microscopy: First steps of metal nanocluster formation in one-dimensional zeolite channels. Nano. Lett. 11, 5537-5541.
Blanford, C.F., Carter, C.B., 2003. Electron radiation damage of MCM-41 and related Materials. Microsc. Microanal. 9, 245-263.
Bursill, L.A., Lodge, E.A., Thomas, J.M., 1980. Zeolitic structures as revealed by high-resolution electron microscopy. Nature, 111-113.
Bursill, L.A., Thomas, J.M., Rao, K.J., 1981. Stability of zeolites under electron irradiation and imaging of heavy cations in silicates. Nature, 157-158.
Casado, C., Amghouz, Z., Garcia, J.R., Boulahya, K., Gonzalez-Calbet, J.M., Tellez, C., Coronas, J., 2009. Synthesis and characterization of microporous titanosilicate ETS-10 obtained with different Ti sources. MRS Bulletin 44, 1225-1231.
Csencsits, R., Gronsky, R., 1987. Damage of zeolite Y in the TEM and its effects on TEM image. Ultramicroscopy, 421.
Díaz, I., Kokkoli, E., Terasaki, O., Tsapatsis, M., 2004. Surface structure of zeolite (MFI) crystals. Chem. Mater. 16, 5226–5232.
Díaz, I., Mayoral, A., 2011. TEM studies of zeolites and ordered mesoporous materials. Micron 42, 512–527.
Egerton, R.F., 2013. Control of radiation damage in the TEM. Ultramicroscopy 127, 100–108.
Egerton, R.F., Li, P., Malac, M., 2004. Radiation damage in the TEM and SEM. Micron 35, 399–409.
Egerton, R.F., McLeod, R., Wang, F., Malac, M., 2010. Basic questions related to electron-induced sputtering in the TEM. Ultramicroscopy 110, 991-997.
Hobbs, L., 1979. Radiolysis and defect structure in electron-irradiated alpha-quartz. Plenum Press, New York.
Hobbs, L.W., 1985. Radiation effects in the electron microscope. EMSA Bull. 15, 51-63.
Kokotailo, G.T., Sawruk, S., Lawton, S.L., 1972. Direct Observation of Stacking Faults ni the Zeolite Erionite. Am. Mineral. 57.
Lu, J., Aydin, C., Browning, N.D., Gates, B.C., 2012. Imaging isolated gold atom catalytic sites in zeolite NaY. Angew. Chem. Int. Ed. 51, 5842-5846.
Mayoral, A., Anderson, P.A., 2007. Production of bimetallic nanowires through electron beam irradiation of copper- and silver-containing zeolite A. Nanotechnology 18, 165708.

Mayoral, A., Carey, T., Anderson, P.A., Diaz, I., 2013a. Atomic resolution analysis of porous solids: A detailed study of silver ion-exchanged zeolite A. Micropor. Mesopor. Mater. 166, 117-122.
Mayoral, A., Carey, T., Anderson, P.A., Lubk, A., Diaz, I., 2011. Atomic Resolution Analysis of Silver Ion-Exchanged Zeolite A. Angew. Chem. Int. Ed. 50, 11230–11233.
Mayoral, A., Coronas, J., Casado, C., Tellez, C., Díaz, I., 2013b. Atomic Resolution Analysis of Microporous Titanosilicate ETS-10 through Aberration Corrected STEM Imaging. Chem. Cat. Chem. 5, 2595–2598.
Mayoral, A., Readman, J.E., Anderson, P.A., 2013c. Aberration-Corrected STEM Analysis of a Cubic Cd Array Encapsulated in Zeolite A. J. Phys. Chem. C 117, 24485−24489.
Menter, J.W., 1958. The electron microscopy of crystal lattices. Adv. Phys., 299-348.
Ortalan, V., Uzun, A., Gates, B.C., Browning, N.D., 2010. Direct imaging of single metal atoms and clusters in the pores of dealuminated HY zeolite. Nature Nanotechnology 5, 506-510.
Readman, J.E., Barker, P.D., Gameson, I., Hriljac, J.A., Zhou, W., Edwards, P.P., Anderson, P.A., 2004. An Ordered Array of Cadmium Clusters Assembled in Zeolite A. Chem. Commun., 736.
Robson, H., Lillerud., K.P., 2001. Syntheses of Zeolitic Materials. 2nd Edition.
Ruan, J., Wu, P., Slater, B., Zhao, Z., Wu, L., Terasaki, O., 2009. Structural Characterization of Interlayer Expanded Zeolite Prepared From Ferrierite Lamellar Precursor. Chem. Mater. 21, 2904–2911.
Sakamoto, Y., Kodaira, T., 2013. Effects of electron beam irradiation on aluminophospate microporous material $ALPO_4$-5. Nucl. Instrum. Methods Phys. Res., Sect. B 315, 197-200.
Terasaki, O., Ohsuna, T., 1995. What can we observe in zeolite related materials by HRTEM? Catal. Today 23, 201-218.
Terasaki, O., Ohsuna, T., 2003. TEM study on zeolite fine structures: homework from Cambridge days. Topics in Catal. 24, 13-18.
Williams, D.B., Carter, C.B., 1996. *Transmission electron microscopy*. (I) Basics, (II) Diffraction, (III) Imaging and (IV) Spectrometry. Plenum, New York.
Yoshida, K., Toyoura, K., Matsunaga, K., Nakahira, A., Kurata, H., Ikuhara, Y.H., Sasaki, Y., 2013. Atomic sites and stability of Cs+ captured within zeolitic nanocavities. Sci. Rep. 2, 2457.